

Size distributions of fine silicate and other particles in Masaya's volcanic plume

R. S. Martin,¹ T. A. Mather,² D. M. Pyle,² M. Power,³ V. I. Tsanev,⁴ C. Oppenheimer,⁴ A. G. Allen,⁵ C. J. Horwell,⁶ and E. P. W. Ward⁷

Received 28 September 2008; revised 11 February 2009; accepted 19 February 2009; published 14 May 2009.

[1] Direct-sampling and remote-sensing measurements were made at the crater rim of Masaya volcano (Nicaragua) to sample the aerosol plume emanating from the active vent. We report the first measurements of the size distribution of fine silicate particles ($d < 10 \mu\text{m}$) in Masaya's plume, by automated scanning electron microscopy (QEMSCAN) analysis of a particle filter. The particle size distribution was approximately lognormal with modal $d \sim 1.15 \mu\text{m}$. The majority of these particles were found to be spherical. These particles are interpreted to be droplets of quenched magma produced by a spattering process. Compositional analyses confirm earlier reports that the fine silicate particles show a range of compositions between that of the degassing magma and nearly pure silica and that the extent of compositional variability decreases with increasing particle size. These results indicate that fine silicate particles are altered owing to reactions with acidic droplets in the plume. The emission flux of fine silicate particles was estimated as $\sim 10^{11} \text{ s}^{-1}$, equivalent to $\sim 55 \text{ kg d}^{-1}$. Sun photometry, aerosol spectrometry, and thermal precipitation were used to determine the overall particle size distribution of the plume ($0.01 < d(\mu\text{m}) < 10$). Sun photometry and aerosol spectrometry measurements indicate the presence of a large number of particles (assumed to be aqueous) with $d \sim 1 \mu\text{m}$. Aerosol spectrometry measurements further show an increase in particle size as the nighttime approached. The emission flux of particles from Masaya was estimated as $\sim 10^{17} \text{ s}^{-1}$, equivalent to $\sim 5.5 \text{ Mg d}^{-1}$ where $d < 4 \mu\text{m}$.

Citation: Martin, R. S., T. A. Mather, D. M. Pyle, M. Power, V. I. Tsanev, C. Oppenheimer, A. G. Allen, C. J. Horwell, and E. P. W. Ward (2009), Size distributions of fine silicate and other particles in Masaya's volcanic plume, *J. Geophys. Res.*, 114, D09217, doi:10.1029/2008JD011211.

1. Introduction

[2] Masaya (elevation $\sim 600 \text{ m}$, Nicaragua, $11^{\circ}59'04'' \text{ N}$, $86^{\circ}10'06'' \text{ W}$) is considered a laboratory volcano by virtue of its vigorous and persistent aerosol plume (emanating from the active Santiago vent) and ease of access due to the extensive local road network which permits remote-sensing and direct-sampling studies of the plume from the crater rim to several kilometers downwind [Stoiber *et al.*, 1986; Horrocks *et al.*, 1999; Burton *et al.*, 2000; Allen *et al.*, 2002; Mather *et al.*, 2003, 2004a; Witt *et al.*, 2008]. This “quiescent” activity has persisted at Masaya for at least the last

150 years (with the current degassing crisis beginning in 1993), and eruptions are rare [Stoiber *et al.*, 1986; Rymer *et al.*, 1998; Duffell *et al.*, 2003]. The plume of Masaya is a mixture of major and minor gases (e.g., H_2O , CO_2 , SO_2 , HCl , HF , HBr , and others), trace gases (e.g., NO_x , HNO_3 , BrO , Hg , and others) and particles (e.g., aqueous droplets, soluble ionic salts, insoluble particles). The extended time periods over which the plume is in contact with the ground (owing to the low elevation of Masaya and gentle slope of the surroundings) leads to deposition of gases and particles over a wide area; in times of enhanced degassing this may lead to a significant environmental impacts (e.g., human respiratory irritation, destruction of vegetation and crops) [Baxter *et al.*, 1982; Stoiber *et al.*, 1986; Delmelle *et al.*, 2001, 2002]. The composition of Masaya's plume is well constrained in terms of gases [e.g., Horrocks *et al.*, 1999; Burton *et al.*, 2000] and soluble particles [Allen *et al.*, 2002; Mather *et al.*, 2003]. However, no attempts have been made to investigate insoluble particles (e.g., fine silicate and reduced S-rich particles) within Masaya's plume.

[3] Fine silicate particles (diameter, $d < 10 \mu\text{m}$; defined to include both crystalline and amorphous grains) have been detected in the quiescent and primarily magmatic plumes of Mount Etna [Lefevre *et al.*, 1986; Martin *et al.*, 2008],

¹Department of Earth Sciences, University of Cambridge, Cambridge, UK.

²Department of Earth Sciences, University of Oxford, Oxford, UK.

³Intellection U.K. Ltd., Conwy, UK.

⁴Department of Geography, University of Cambridge, Cambridge, UK.

⁵Analytical Chemistry Department, Chemistry Institute, Sao Paulo State University, Sao Paulo, Brazil.

⁶Institute of Hazard and Risk Research, Department of Earth Sciences, Durham University, Durham, UK.

⁷Department of Materials Science and Metallurgy, University of Cambridge, Cambridge, UK.

Table 1. Summary of Techniques Used in This Study^a

Technique	Component Measured	Time Resolution	Nature of Technique
Thermal precipitator (+ STEM)	all particles, $0.01 < d(\mu\text{m}) < 0.1$	60 min	direct sampling
Sun photometry	all particles, $0.08 < d(\mu\text{m}) < 4$	6 s	remote sensing
Aerosol spectrometry	all particles, $0.35 < d(\mu\text{m}) < 10$	1 min	direct sampling
Particle filters (+ QEMSCAN)	silicate particles, $0.5 < d(\mu\text{m}) < 10$	30 min	direct sampling
Acid gas filters (+ IC)	gaseous SO ₂	30 min	direct sampling
UV spectroscopy	gaseous SO ₂	15 s	remote sensing

^aSTEM, scanning transmission electron microscopy; QEMSCAN, automated scanning electron microscopy; IC, ion chromatography.

Kilauea [Meeker and Hinkley, 1993], and Popocatepetl [Obenholzer et al., 2003]. In addition, fine silicate particles have also been detected within fumarolic emissions (e.g., Poás, Costa Rica [Pfeffer et al., 2006]). Fine silicate particles in quiescent plumes may be produced by a range of different processes, including magma spattering (above fluid, high-temperature lava surfaces), condensation from Si-rich vapors and the suspension of fragments of wall rock and/or fumarolic encrustations into the passing gas flow. The emission of fine silicate particles during quiescent degassing is distinct from the emission of volcanic ash during eruptions, which is formed by explosive fragmentation of the magma. As we shall show, fine silicate particles have a much narrower size distribution than volcanic ash. On the basis of our new work and on comparisons with the few documented examples of similar fine silicate particles from elsewhere, we suggest that the size, shape, and composition of these particles may provide useful information about premission, synmission, and postmission processes close to the magma-air interface during quiescent volcanic activity.

[4] In this study, we use automated scanning electron microscopy to calculate the size, shape and compositional distributions of fine silicate particles in Masaya's plume which were collected onto a particle filter by air filtration [e.g., Mather et al., 2003]. We also consider the size distribution of reduced S-rich particles (e.g., sulfur and sulfides) in Masaya's plume. These results are complemented by overall size distributions of particles in the plume measured by Sun photometry [Watson and Oppenheimer, 2000, 2001; Mather et al., 2004c; Porter et al., 2002] and aerosol

spectrometry [Mather et al., 2004b; Allen et al., 2006]. Samples were also collected using a thermal precipitator [Maynard, 1995] and analyzed using scanning transmission electron microscopy (STEM) to estimate the size distribution of nanoparticles in the plume. Ion chromatographic (IC) analysis of acid gas filters [e.g., Mather et al., 2003, 2006a] and UV differential optical absorption spectroscopy (DOAS) [McGonigle et al., 2002, 2003; Galle et al., 2003] were used to measure SO₂ in the plume (i.e., the concentration of SO₂ at the crater rim and total column SO₂, respectively) allowing particle emission fluxes to be estimated from the calculated size distributions. The sampling techniques used in this study are summarized in Table 1 (where appropriate, with the information on the particle size range measured by each technique). All measurements were made in November to December 2003 except the thermal precipitator sample, which was collected in March 2006.

[5] This combination of sampling and analytical techniques allows for a comprehensive survey of particles in Masaya's plume with special reference to types of particles not considered by earlier studies (e.g., fine silicate particles, reduced S-rich particles, and nanoparticles). This study offers an improved understanding of the composition of Masaya's plume and enhances assessments of the environmental, atmospheric, and human impacts of active volcanism.

2. Sample and Measurement Locations

[6] Measurement locations were selected in order to sample and characterize the aerosol plume emanating from

Table 2. List of Samples^a

Sample	Date	Sampling Period (Local Time)	Number of Measurements (<i>m</i>)	Standard Error of Mean (%)
GM01	20 Nov 2003	0933–1006	33	3.5
GM02	20 Nov 2003	1244–1348	64	2.5
GM03	21 Nov 2003	1512–1658	106	1.9
GM04	22 Nov 2003	0917–0951	34	3.4
GM05	22 Nov 2003	1512–1757	165	1.6
GM06	23 Nov 2003	0719–0918	119	1.8
GM07	26 Nov 2003	1107–1225	78	2.3
GM08	26 Nov 2003	1439–1645	126	1.8
GM09	2 Dec 2003	1015–1045	30	3.7
SP01	22 Nov 2003	0915–0930	150	0.8
SP02	27 Nov 2003	1331–1342	110	1.0
SP03	2 Nov 2003	1015–1045	290	0.6
SP04	3 Nov 2003	0955–1000	50	1.4
UV01	2 Dec 2003	1015–1045	120	0.5
QM04/IC04	29 Nov 2003	0925–0952	1	-
TP01	1 Mar 2006	0944–1044	1	-
TP02	1 Mar 2006	1105–1205	1	-
TP03	2 Mar 2006	1018–1118	1	-

^aGM, aerosol spectrometry; SP, Sun photometry; QM, particle filter; UV, differential optical absorption spectroscopy; IC, acid gas filter; TP, thermal precipitation. Standard errors of the mean are calculated on the basis of analytical uncertainties on a single measurement and the number of measurements (*m*).

the active Santiago vent at Masaya. All locations were on the crater rim, typically ~ 200 m above the active vent. During the campaigns (in 2003 and 2006), the plume could be observed escaping from a decimeter-scale vent, which was incandescent at night, and presumed to be the opening to a subterranean lava pool by comparison with extended observations at Masaya over the past 20 years [Rymer *et al.*, 1998]. The plume age at the time of sampling was estimated to be < 1 min on the basis of timing the transport of “puffs” from the active vent to the measurement location. The activity of Masaya during both campaigns was characterized by quiescent degassing punctuated by several small but audible explosions. The frequency of the explosions varied from several events per minute to once every few hours. The explosions were not ash-forming (i.e., no darkening of the plume was observed) and were most likely caused by the arrival of large gas bubbles at the top of the conduit. While the level of the magma was higher in the conduit in 2003 than in 2006, the SO_2 flux ($\sim 40 \text{ mol s}^{-1}$) and mean $[\text{SO}_2]$ at the crater rim ($200 \mu\text{mol m}^{-3}$) were comparable between campaigns [Mather *et al.*, 2006a; Witt *et al.*, 2008]. Temperature and relative humidity were monitored throughout the campaigns and confirm previous studies [e.g., Mather *et al.*, 2003] showing that decreasing temperatures (i.e., toward the nighttime) generally correspond to increasing relative humidity, which results in plume condensation.

[7] Samples are labeled with a prefix (aerosol spectrometer, GM; Sun photometer, SP; acid gas filter, IC; particle filter, QM; thermal precipitator, TP; differential optical absorption spectroscopy, UV) and sample number. Sample details (including analytical uncertainties) are given in Table 2.

3. Methodology

3.1. Field Sampling and Measurements

3.1.1. Filter Packs (QM + IC)

[8] The aerosol plume was sampled by pumping ambient air through a filter pack. The filter pack used consisted of a particle filter (Millipore, 47 mm, AAWP, pore size $0.8 \mu\text{m}$) followed by three acid gas filters (Whatman 41 ashless circles each impregnated with 10% NaHCO_3 and 1% glycerol in 1:1 methanol/distilled deionized water) housed in a multiple-stage cartridge. Acidic gases (SO_2 , HCl , HF , HNO_3) are converted to the weakly basic counter-anions ($\text{SO}_3^{2-}/\text{SO}_4^{2-}$, Cl^- , F^- and NO_3^-) with good efficiency [Mather *et al.*, 2003]. The initial and final flow rates through the filter pack were measured (17 L min^{-1} , in both cases) allowing the total volume of air sampled to be calculated. After collection, filters were triple-sealed in individual plastic bags and stored in a freezer to prevent further reaction.

3.1.2. Sun Photometry (SP)

[9] The direct solar radiance through the plume was measured at wavelengths of 440, 675, 870, 936, and 1020 nm using a handheld Microtops II Sun photometer [Morys *et al.*, 2001]. The channels' peak wavelength precision is ± 1.5 nm, the full-width-at-half-maximum is 10 nm, and the field of view is 2.5° . Data are automatically recorded and handled by a built-in microprocessor which calculates the total optical thickness, τ_{tot} , averaged over a time period of 6 s. Measurements were also made in background air (i.e., air assumed to be free from local volcanic influences) before and after each set of plume measurements to determine the background

optical thickness, τ_{bg} . The background optical thickness was then subtracted from the total optical thickness, τ_{tot} , to give the plume aerosol optical thickness (i.e., $\tau_{\text{plume}} = \tau_{\text{tot}} - \tau_{\text{bg}}$). The scattering of light by gases within the plume (i.e., Rayleigh scattering) is a negligible contribution to τ_{tot} (since gases do not scatter significantly over small path lengths, i.e., the plume thickness) and may be disregarded [e.g., Watson and Oppenheimer, 2001].

[10] Data were preprocessed to remove any scans that had not completed, or scans which generated clearly erroneous numbers. The data were retrieved through an iterative inversion procedure (using software described by Mather *et al.* [2004c] and V. I. Tsanev and T. A. Mather, Microtops Inverse: Software package for retrieving aerosol columnar size distributions using Microtops II data, available at <http://www.fsf.nerc.ac.uk>, 2007) that estimates a particle size distribution ($0.08 < d(\mu\text{m}) < 4$) on the basis of the calculated plume aerosol optical thickness, the uncertainties of these measurements, and the index of refraction. We assume that the particles are spherical aqueous sulfate aerosols which scatter but do not absorb light with a complex index of refraction of $n = 1.44 + 0 i$ for 440–1020 nm [Watson and Oppenheimer, 2001]. The estimated particle size distribution is then used to predict the plume aerosol optical thickness which is compared with the measurements. In an “ideal” retrieval, successive iterations would converge to a particle size distribution which reproduces the plume aerosol optical thickness to within measurement uncertainty (i.e., $< 0.1\%$ in each channel). However, all retrievals with agreements better than 10% were accepted. A similar approach was used by Watson and Oppenheimer [2001], where a threshold of 5% was used. The uncertainties in the particle size distribution (i.e., $< 10\%$) are small compared to the inherent variability at the crater rim due to plume dilution and puffing [Branan *et al.*, 2008]. Standard errors of the mean (due to the analytical uncertainties) were estimated using $0.1/\sqrt{m}$, where m is the number of measurements (Table 2).

3.1.3. Aerosol Spectrometry (GM)

[11] Total aerosol number concentrations were measured using GRIMM Aerosol Technik GmbH (Ainring, Germany) Aerosol Spectrometer (Model 1.106). The plume was sampled by pumping the ambient air (at 1.2 L min^{-1}) through a detector cell containing a semiconductor laser light source (780 nm), generating a scattered light signal proportional to the size of the aerosol particle causing the light scatter. A receptor diode collects the 90° scattered light, the signal being processed in a multichannel size classifier. The optics are protected against contamination using a sheath airflow. The aerosol spectrometer recorded volumetric particle concentrations in eight size ranges: > 0.35 , > 0.5 , > 0.75 , > 1.0 , > 2.0 , > 3.5 , > 5 , and $> 6.5 \mu\text{m}$. The upper limit of all size ranges was approximated to $10 \mu\text{m}$. Data were collected continuously as 1-min averages. Measurements were also made in background air before and after each set of plume measurements to allow the concentrations of nonvolcanic particles in each size range to be subtracted. The data-processing software (Grimm 1.174) assumes spherical particles with $n = 1.59 - 0 i$ (at 780 nm); this index of refraction is fixed and cannot be changed by the user. Previous studies [King, 1982; Martinez-Lozano *et al.*, 1999] indicate that the retrieved size distributions are not highly sensitive to

the real part of the index of refraction. However, uncertainties in the imaginary part of the index of refraction may lead to smoothing or exaggeration of sharp features (e.g., local maxima in the size distribution). The uncertainty on a single measurement (i.e., the concentration of particles within each size range) was estimated as $\sim 20\%$ on the basis of 40 measurements made in background air (the true uncertainty may be much less if the variability in background air is due to heterogeneity rather than analytical uncertainties). In any case, this uncertainty is small compared to the inherent variability in the measurements. Standard errors of the mean (due to the analytical uncertainties) are estimated using $0.2/\sqrt{m}$, where m is the number of measurements (Table 2).

3.1.4. Differential Optical Absorption Spectroscopy (UV)

[12] DOAS measurements of SO_2 column amounts (toward the zenith) were made with an Ocean Optics Inc. USB2000 spectrometer [Galle *et al.*, 2003]. Measurements were made in stationary mode and complement traverse mode measurements made on the same campaign [Mather *et al.*, 2006a]. SO_2 column amounts were determined at ~ 15 -s intervals, with an analytical uncertainty of $\sim 5\%$ [Mather *et al.*, 2006a]. Standard errors of the mean (due to the analytical uncertainties) are estimated using $0.05/\sqrt{m}$, where m is the number of measurements (Table 2).

3.1.5. Thermal Precipitation (TP)

[13] The plume was sampled by pumping the ambient air (at 1 L min^{-1}) through a thermal precipitator [Maynard, 1995]. The instrument produces a thermal gradient between two plates ($\Delta T = 100 \text{ K}$, $\nabla T = 10^6 \text{ K m}^{-1}$) causing deflection of the particles in a direction perpendicular to the flow and resulting in deposition onto a 3-mm-diameter carbon-coated Ni grid (Agar Scientific, UK). The deposition efficiency is independent of particle size between 0.004 and $\sim 0.04 \mu\text{m}$ and becomes less efficient at higher particle diameters. After collection, samples were placed in a grid box and stored in the freezer to prevent further reaction. This sampling technique has been previously applied to Mount Etna volcano [Martin *et al.*, 2008].

3.2. Laboratory Analyses

3.2.1. QEMSCAN

[14] The particle filter from the filter pack was analyzed using automated scanning electron microscopy (QEMSCAN [Pirrie *et al.*, 2004; Martin *et al.*, 2008]) to determine the size, shape, and composition of 5037 particles on the filter. To prepare the sample for analysis, a 25-mm diameter circle was cut from the particle filter (to fit the mount) and coated with carbon to a thickness of 25 \AA . Following preparation, the sample was loaded into the QEMSCAN instrument and the analysis was initiated using the control program (iDiscover, Intellection). Particles with diameters between 0.2 and $10 \mu\text{m}$ were automatically located and sized using the contrast in the backscattered electron signal between particles and the filter. Subsequently, four energy dispersive X-ray (EDX) spectrometers acquired spectra from each particle with a beam stepping interval (i.e., spacing between acquisition points) of $0.2 \mu\text{m}$, an accelerating voltage of 25 keV , and a beam current of 5 nA . Interactions between the beam and the sample were modeled through Monte Carlo simulation; this simulation allows the collection of spectra to be performed at a higher resolution than the beam width ($\sim 2 \mu\text{m}$). The EDX

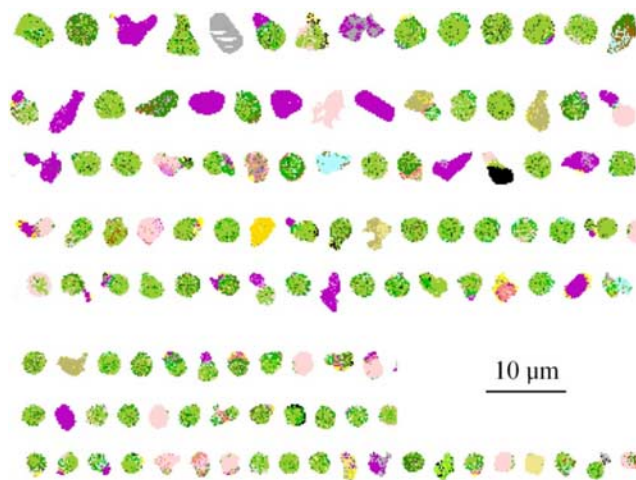


Figure 1. An excerpt from the QM04 particle index file (which is grouped according to size). The coloring of each pixel denotes the assigned composition. This excerpt is for demonstration purposes only and is not representative of the whole sample.

spectra were compared with spectra held in a look-up table allowing an assignment to be made of a composition at each acquisition point. The look-up table contains entries for silicate, S-rich and chloride species (Table 3). The assignment makes no distinction between mineral species and amorphous grains of similar composition. The presence of elements other than those listed in Table 3 does not affect the assignment. This procedure allows a compositional map of the particle to be generated. These compositional maps were output as an index file where each particle is represented by a scaled image (scale of $0.2 \mu\text{m pixel}^{-1}$) with pixel coloring denoting the assigned composition (e.g., Figure 1). Image analysis software (ImageJ [Abramoff *et al.*, 2004]) was used to fit an ellipse (with equivalent area, centroid, and orientation) to each particle in the index file and to output results to a spreadsheet. The major, $a(\mu\text{m})$, and minor, $b(\mu\text{m})$, axes of each ellipse were used to calculate an equivalent particle diameter from $d = \sqrt{(ab)}$ (in units of μm). To allow investigation of the relationships between particle size and shape, entries in the spreadsheet pertaining to fine silicate particles were identified by inspection of the compositional map.

[15] Results were also output by the QEMSCAN software as a spreadsheet giving the weight percent (wt%) of each composition in the look-up table (Table 3) at $1\text{-}\mu\text{m}$ particle size intervals (i.e., for $0\text{--}1 \mu\text{m}$, $1\text{--}2 \mu\text{m}$, etc.). These results are semiquantitative because the weight percent of each composition was calculated from the compositional assignments (rather than the original EDX spectra) using an approximate stoichiometry for each composition. This approach reflects the design of the instrument which is optimized for rapid compositional identification rather than detailed compositional analysis (for which other techniques are more appropriate). The silicate compositions were grouped into “metal-rich” (all identified phases of the form M-Si-O) and “metal-poor” (Si-O). An assignment of the latter implies that the intensity of EDX signals attributable to metals were small, hence metal-poor is synonymous with nearly pure silica (the terminology of Lefevre *et al.* [1986]). We define the parameter Z to equal (Si-O

Table 3. Look-up Table for QEMSCAN^a

Composition	Type
Si-O	metal-poor silicate
Na-K-Al-Si-O	metal-rich silicate
Ca-Na-Al-Si-O	metal-rich silicate
Fe-Al-Si-O	metal-rich silicate
Ca-Fe-Si-O	metal-rich silicate
Ca-Al-Si-O	metal-rich silicate
Mg-Fe-Al-Si-O	metal-rich silicate
Mg-Fe-Si-O	metal-rich silicate
Ca-S-O	oxidized S-rich
Al-S-O	oxidized S-rich
Fe-S-O	oxidized S-rich
Fe-Al-S-O	oxidized S-rich
K-S-O	oxidized S-rich
Al-S-O	oxidized S-rich
Na-S-O	oxidized S-rich
Na-K-S-O	oxidized S-rich
Na-Mg-Fe-S-O	oxidized S-rich
S	reduced S-rich
Fe-S	reduced S-rich
Cl	chloride

^aThe assignment does not distinguish between mineral and amorphous species of similar composition. The presence of elements other than those listed does not affect the assignment.

wt%)/(Si-O wt% + M-Si-O wt%) within each size interval. The limits of $Z = 0$ and $Z = 1$ denote metal-rich and metal-poor end-members, respectively. While the relationship between Z and mean SiO_2 wt% (for particles in each size interval) cannot be stated exactly (because the composition of particles were not analyzed fully), the metrics are clearly positively correlated.

3.2.2. Scanning Transmission Electron Microscopy (STEM)

[16] Images of particle fields on the Ni grids collected via thermal precipitation were acquired using a Tecnai F20 microscope operated at 200 keV by scanning a narrow probe of electrons across the sample and recording the intensity of the transmitted electrons scattered to high angles using a high-angle annular dark field detector. The near-vacuum operational pressure of the instrument likely results in the evaporation of liquid droplets. Hence, the particles imaged are either deposited as solids, or as liquids which evaporate during storage or analysis to form precipitates. Particle fields of area $\sim 4 \mu\text{m}^2$ were selected randomly and imaged. Each image was then processed with image analysis software (ImageJ) to subtract the background and enhance contrast. This processing was followed by thresholding to produce an image of particles (black) on a white background. Threshold limits were chosen using the onset of inclusion of background shown by a marked increase in the number of dark pixels. Image analysis was then used to generate a spreadsheet containing size data for each particle (as described in section 3.2.1). To allow for uneven particle deposition on the grid, several particle fields were analyzed from each sample. Particles with diameter $d < 0.01 \mu\text{m}$ were ignored as genuine particles and errant pixels (an artifact of image processing) could not be reliably distinguished.

3.2.3. Ion Chromatography (IC)

[17] The acidic gas filters (IC04) were analyzed using ion chromatography as part of a larger set of acidic gas filter samples collected at Masaya by *Mather et al.* [2006a]. The results for each set of filters were not given individually, and we now report that analysis of IC04

showed the mean $[\text{SO}_2]$ in plume pumped through the filter pack was $(183 \pm 38) \mu\text{mol m}^{-3}$.

3.3. Data Elaboration

[18] Particle size distributions are described by a number density distribution, $N(d)$ (m^{-3}), as given in equation (1) [e.g., *Allen et al.*, 2006; *Martin et al.*, 2008]. Integration of $N(d)$ yields the number of particles per cubic meter, dN (m^{-3}), with diameters, $d(\mu\text{m})$, between the limits:

$$N(d) = \frac{dN}{d \log(d)}. \quad (1)$$

For the retrieval of $N(d)$ from image analysis data (i.e., QEMSCAN and STEM), we first calculate the number density distribution of imaged particles, $M(d)$ (unitless) as given by equation (2), where dM is the number of particles detected within each size interval of width $d \log(d)$:

$$M(d) = \frac{dM}{d \log(d)}. \quad (2)$$

For QEMSCAN data, $N(d)$ can be calculated from $M(d)$ by dividing by the area fraction of filter analyzed, A (unitless) (i.e., $A = 0.05$ if 5% of the filter is analyzed), and the volume of plume sampled, V_p (m^3) (equation (3a)). For STEM data, $N(d)$ can be calculated from $M(d)$ by dividing by the area of grid analyzed, B (m^2), the sampling duration, t (s), and the theoretical deposition flux of the thermal precipitator ($D = 0.03 \text{ m s}^{-1}$ [*Maynard*, 1995]) (equation (3b)):

$$N(d) = \frac{1}{AV_p} M(d), \quad (3a)$$

$$N(d) = \frac{1}{BDt} M(d). \quad (3b)$$

Sun photometry results are output by the inversion software as a column number density distribution, $C(d)$ (m^{-2}). $N(d)$ can be estimated from $C(d)$ by dividing by the plume thickness along the line of sight of the instrument, L (m) (equation (4)). The average plume thickness was estimated as ~ 10 – 100 m on the basis of observations made at the time of measurement; in calculations, we use the geometric midpoint of the estimated range, $L = 32$ m. The uncertainty on L does not affect the shape of $N(d)$:

$$N(d) = \frac{1}{L} C(d). \quad (4)$$

Aerosol spectrometry results are output by the data-processing software in a form equivalent to the integral of $N(d)$ between one of eight lower limits (e.g., $0.35 \mu\text{m}$, $0.5 \mu\text{m}$, and so on) and $10 \mu\text{m}$. These results must be first differenced and then differentiated with respect to $\log(d)$ to obtain $N(d)$ (where d is taken as the geometric mean of the limits). Particle size distributions may also be described by the volume density distribution, $V(d)$ ($\mu\text{m}^3 \text{ m}^{-3}$). $V(d)$ can be estimated from $N(d)$ by assuming that particles are spherical [*Watson and Oppenheimer*, 2001]:

$$V(d) = \frac{\pi}{6} d^3 N(d). \quad (5)$$

Particle shape distributions are described by the elongation, E (unitless) [e.g., *Martin et al.*, 2008]:

$$E = 1 - \frac{b^2}{a^2}. \quad (6)$$

4. Results and Discussion

4.1. Silicate Particles

[19] The fine silicate particles collected at Mount Etna [*Lefevre et al.*, 1986] and Kilauea [*Meeker and Hinkley*, 1993] were predominantly spherical, with modal $d \sim 1 \mu\text{m}$ and were considered to be primary particles emitted directly by the magma. These particles exhibit a range of compositions between that of the degassing magma (typically basaltic, in both cases) and nearly pure silica. This compositional variability is most likely due to the reaction of silicate particles with acidic droplets in the plume [*Spadaro et al.*, 2002; *Moune et al.*, 2007; *Delmelle et al.*, 2007]. These results were verified by recent and more systematic studies using QEMSCAN analysis of fine silicate particles in the Mount Etna plumes [*Martin et al.*, 2008] although a significant proportion of the particles were found to be nonspherical. The mechanism by which fine silicate particles form is not known, but our working hypothesis is that they form during bubble bursting at the magma surface [*Martin et al.*, 2008]. By analogy with the formation of the sea-spray aerosol [*Spiel*, 1998], the bursting of small gas bubbles as they reach the magma surface will form a fine spray of particles, which form by rupture of the melt film that encloses the bubble. This mechanism is a low-energy process, and quite distinct from the energetic fragmentation processes that usually accompany the formation of volcanic ash particles. The size distributions of particles generated by this mechanism in salt water and other liquids (e.g., molten iron) [*Russell and Singh*, 2006; *Han and Holappa*, 2001, 2003; *Lewis and Schwartz*, 2004] are typically lognormal with modal diameter $\sim 1 \mu\text{m}$, consistent with the size distribution of fine silicate particles found by *Martin et al.* [2008]. The presence of fine silicate particles in fumarolic emissions [e.g., *Pfeffer et al.*, 2006] indicates that Si-rich particles may also be formed by secondary processes (e.g., condensation of Si-rich vapor). A further possibility is that fine silicate particles are formed by the suspension of fragments of wall rock and/or fumarolic encrustations [*Obenholzner et al.*, 2003]. There is no evidence to suggest that these scenarios are relevant to Masaya's quiescent plume, not least because there is minimal fumarolic activity within the Santiago crater.

[20] In sections 4.1.1–4.1.3, we present size, shape, and compositional distributions for particles collected on QM04 (Table 2). QM04 constitutes independent analyses of 5037 particles, of which 3453 were identified as fine silicate particles. By the law of large numbers, we may expect these distributions to be well characterized for the sample [e.g., *Pirrie et al.*, 2009]. Masaya exhibits a spectrum of quiescent activity (i.e., varying frequency of explosions, varying level of magma in the conduit), and QM04 may not be representative of all activity at Masaya. However, this sample was selected for QEMSCAN analysis because (1) the SO_2 concentration measured from the acid gas filter (ICO4) was close to the average for the campaign [*Mather et al.*, 2006a]

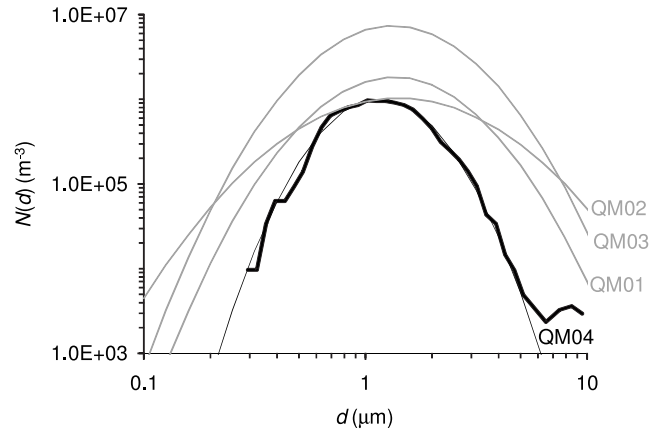


Figure 2. Number density distribution, $N(d)$, from automated scanning electron microscopy (QEMSCAN) measurements (black solid line) and lognormal fit (gray thin line) for fine silicate particles in Masaya's plume (QM04). Lognormal fits to the $N(d)$ for fine silicate particles in the Mount Etna plumes (QM01–QM03 [*Martin et al.*, 2008]) are given for comparison. The parameters of $N(d)$ are given in Table 4.

and (2) there were no other indications of atypical activity during the day of measurement (29 November 2003). We may therefore consider results derived from QM04/ICO4 as being a representative average for the 2003 campaign.

4.1.1. Particle Size

[21] The number density distribution of fine silicate particles (i.e., Si-O and M-Si-O), $N(d)$, in the plume of Masaya was approximately lognormal (equation (7)) with modal diameter $d^*_N \sim 1.15 \mu\text{m}$. The lognormal distribution is defined by the parameters N' , σ_N and μ_N . N' (m^{-3}) denotes the total number of fine silicate particles per cubic meter of air. The parameters σ_N and μ_N are unitless and equivalent to the mean and standard deviation of $N(d)$ in $\log(d)$ space:

$$N(d) = \frac{N'}{\sigma_N \sqrt{2\pi}} \exp\left(-\frac{1}{2} \left(\frac{\log(d) - \mu_N}{\sigma_N}\right)^2\right). \quad (7)$$

Figure 2 shows the results for QM04 with the lognormal fit calculated over the range $0.5 < d(\mu\text{m}) < 5$. These results show that both metal-rich and metal-poor fine silicate particles are components of a single lognormal size distribution. This result indicates that fine silicate particles are formed by a single process, and suggests that the metal-poor particles are formed by alteration of metal-rich particles after emission. Deposition and coagulation of particles in the range $0.5 < d(\mu\text{m}) < 5$ must be minor so as to not introduce significant asymmetry into $N(d)$; consistent with the majority of fine silicate particles being within the aerodynamically stable accumulation mode (i.e., $0.1 < d(\mu\text{m}) < 2$ [*Whitby*, 1978]). $N(d)$ over the range $6 < d(\mu\text{m}) < 10$ is greater than expected by extension of the lognormal distribution from smaller particle size. While this result may indicate an additional resuspended contribution (i.e., from fine silicate particles that had previously been deposited in the crater), it is difficult to draw conclusions as only five particles were detected in this range. These new results add further weight to the general hypothesis introduced by *Martin et al.* [2008] that fine silicate particles are primary particles formed by bubbles

Table 4. Parameters of the Lognormal Number Density Distribution, $N(d)$, and the Volume Density Distribution, $V(d)$, for QM04^a

Sample	Location	N' (m^{-3})	μ_N	σ_N	d_N^*	V' ($\mu\text{m}^3 \text{m}^{-3}$)	μ_V	σ_V	d_V (μm)
QM01	Etna/NEC	1.2×10^6	0.14	0.25	1.38	7.3×10^6	0.57	0.25	3.73
QM02	Etna/VOR	9.0×10^5	0.15	0.36	1.41	2.9×10^7	1.05	0.36	11.1
QM03	Etna/VOR	5.4×10^6	0.14	0.25	1.38	3.3×10^7	0.58	0.25	3.73
QM04	Masaya	5.0×10^5	0.06	0.20	1.15	1.0×10^6	0.34	0.20	2.17

^aResults for QM01–QM03 are presented for comparison. N' denotes the total number of particles per cubic meter. The parameters μ_N and σ_N (both are unitless) are equivalent to the mean and standard deviation of $N(d)$ in $\log(d)$ space, with $\mu_N = \log d_N^*$. The parameters V' , μ_V , d_V^* , and σ_V are defined equivalently in terms of $V(d)$. NEC, North East Crater; VOR, Voragine.

bursting at the surface of the magma. Note that $N(d)$ of the fine silicate particles shown in Figure 2 cannot explain observations of Pele's tears with $d \sim 200 \mu\text{m}$ [Moune *et al.*, 2007], collected from close to the vent, within the main Santiago crater. This indicates that the production of larger silicate particles during quiescent activity is mechanistically distinct from the production of fine silicate particles.

[22] Figure 2 also shows lognormal fits for fine silicate particles in the plumes of Mount Etna, Sicily (QM01–QM03), for comparison [Martin *et al.*, 2008]. This comparison is valid because both Masaya and Mount Etna sustain a persistent aerosol plume through an open vent (although Mount Etna has multiple active vents compared to one at Masaya). Quiescent activity at Mount Etna is interspersed with sporadic summit and flank eruptions; however, the samples were collected from the North East Crater (QM01, August 2005) and Voragine vents (QM02, August 2005, and QM03, July 2004) during periods when the activities of the vents were superficially comparable to the active Santiago vent of Masaya (i.e., quiescent degassing with small but audible explosions). The differences between $N(d)$ for Masaya and Mount Etna fine silicate particles can be seen most clearly in Table 4, which shows σ_N , μ_N , and d_N^* are significantly smaller at Masaya. This result suggests differences in the processes forming fine silicate particles at Mount Etna and Masaya, perhaps related to differences in the size distributions of bubbles in the magma, bubble overpressure, and/or magma viscosity (by analogy with bubble bursting in other systems [Lewis and Schwartz, 2004; Han and Holappa, 2001, 2003]). The similarities in σ_N and μ_N between samples collected at Mount Etna (relative to the differences with QM04) may suggest that σ_N and μ_N (generally) are related to longer-term geophysical parameters, and so are not subject to a significant degree of short-term fluctuation (cf., if σ_N and μ_N did vary significantly from one day to the next, it would be highly coincidental that all three samples from Mount Etna were so similar). This result adds weight to our assumption that QM04 can be taken as representative for the 2003 campaign at Masaya. Further work will offer new insights into the factors affecting $N(d)$ (i.e., σ_N and μ_N) and the origin of fine silicate particles in volcanic plumes.

[23] Multiplying $N'/[\text{SO}_2]$ (where $[\text{SO}_2] = 183 \mu\text{mol m}^{-3}$, i.e., the mean concentration of SO_2 in the plume pumped through the filter pack from section 3.2.3) by the emission flux of SO_2 at the time of sampling (40 mol s^{-1} [Mather *et al.*, 2006a]) yields an emission flux of fine silicate particles from Masaya of $\sim 10^{11} \text{ s}^{-1}$. The scaling assumes that the duration of the sample ($\sim 30 \text{ min}$) was sufficiently long to obtain a representative average value for $N'/[\text{SO}_2]$ without implication that N' and $[\text{SO}_2]$ are correlated on shorter time scales. Degassing from Masaya's magma involves a broad spec-

trum of behavior, from continuous degassing (i.e., large numbers of small bubbles) to discrete explosions (i.e., small numbers of larger bubbles). The result that $N(d)$ is unimodal (Figure 2) indicates that the majority of fine silicate particles in Masaya's plume were formed by a single process. Of course, in the absence of an exact understanding of the formation process of these fine silicate particles, it would seem likely that the full spectrum of degassing modes contributes to $N(d)$. It is difficult to envisage how the discrete explosions could be the main contributor to the calculated emission flux, as this would require each explosion to generate $> 10^{14}$ particles (assuming that a maximum of two explosions occurred during the sampling period; the exact number was not recorded). Thus, continuous degassing likely plays at least a significant role in the origin of the fine silicate particles (as suggested by Martin *et al.* [2008]).

[24] The volume density distribution, $V(d)$, is also lognormal (equation (8)). The parameters of $V(d)$ (σ_V , μ_V , d_V^* , V') are defined analogous to the parameters of $N(d)$ and can be derived from σ_N , μ_N and N' with the relationships given by Martin *et al.* [2008]:

$$V(d) = \frac{V'}{\sigma_V \sqrt{2\pi}} \exp\left(-\frac{1}{2} \left(\frac{\log(d) - \mu_V}{\sigma_V}\right)^2\right). \quad (8)$$

Results are given in Table 4. The volume-weighted modal diameter (d_V^*) indicates that 50% of the total volume of fine silicate particles at Masaya lies below $2 \mu\text{m}$. In contrast, only 1% of the total volume of (a typical) volcanic ash lies below $2 \mu\text{m}$ [Horwell, 2007]. The ratio $V'/[\text{SO}_2] = 5.6 \times 10^9 \mu\text{m}^3 \text{mol}^{-1}$ suggests a fine silicate particle mass flux from Masaya of $\sim 55 \text{ kg d}^{-1}$ (assuming a density of 2800 kg m^{-3} [Lefevre *et al.*, 1986]). If a lognormal distribution is not assumed (i.e., V' is calculated directly from the data, rather than the lognormal parameters of $N(d)$), we estimate a flux of $\sim 60 \text{ kg d}^{-1}$. The comparability between the two estimates indicates that the nonlognormal and poorly constrained part of $N(d)$ (i.e., $6 < d(\mu\text{m}) < 10$) does not introduce large uncertainties into the fine silicate particle mass flux. The fine silicate particle mass flux from Mount Etna is $\sim 7000 \text{ kg d}^{-1}$. The lesser mass flux at Masaya is explained by the lower gas flux as $V'/[\text{SO}_2]$ is similar at both volcanoes. The human impacts of these fluxes are unclear. Although the in-vivo reactivity of fine silicate particles has not yet been established, these particles are small enough to enter the alveolar region [Horwell and Baxter, 2006]. Fine silicate particles should therefore be considered a potential respiratory hazard.

4.1.2. Shape

[25] Figure 3 shows a frequency density distribution for elongation (equation (6)) in fine silicate particles in the

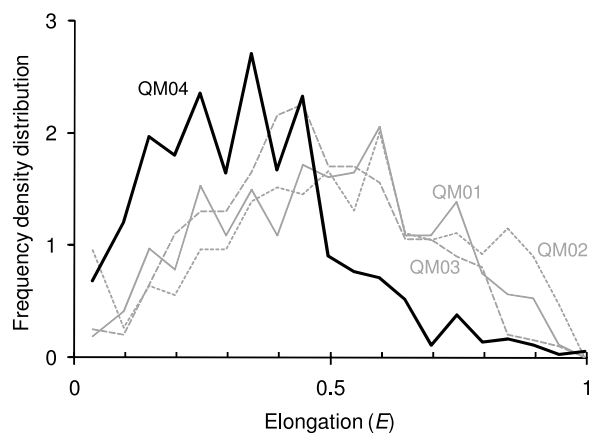


Figure 3. Elongation frequency density distributions for fine silicate particles in the plumes of Masaya (QM04) and Mount Etna (QM01–QM03 [Martin *et al.*, 2008]).

Masaya plume (QM04). Also shown is elongation for fine silicate particles in the Mount Etna plumes (QM01–QM03 [Martin *et al.*, 2008]). A high proportion of fine silicate particles in the Masaya plume were found to be very nearly spherical with modal $E \sim 0.3$. In contrast, the fine silicate particles from Mount Etna show much greater variability in particle shape (with modal $E \sim 0.6$). Wohletz and McQueen [1984] observed the formation of spherical droplets along with a much larger component of fragmental ash during experimental simulations of phreatomagmatic activity. These results may reflect some proportion of the molten ejecta relaxing to a spherical shape (to minimize surface area) prior to quenching. We therefore postulate that the time scale over which particles remain molten is greater at Masaya than at Mount Etna (indicating that dilution of magmatic gases occurs more rapidly in the latter case). These arguments have parallels with textural analyses of eruptive products to infer conditions in the conduit and eruption column [e.g., Zimanowski *et al.*, 2003; Taddeucci *et al.*, 2004, 2007; Polacci *et al.*, 2006].

4.1.3. Composition

[26] Figure 4 shows that Z (which is positively correlated with mean SiO_2 wt%) decreases with increasing particle size. This result shows that smaller fine silicate particles are more significantly depleted in metals than larger fine silicate particles. Similar trends for Z were shown by Martin *et al.* [2008] for fine silicate particles in Mount Etna's plume, suggesting a commonality. We interpret the trends in Z as being consistent with alteration of the fine silicate particles by reaction with acidic droplets in the plume [e.g., Moune *et al.*, 2007; Delmelle *et al.*, 2007]. The smallest particles undergo the most complete alteration because an increased proportion of the total mass lies close to the particle surface ensuring a greater exposure to acidic droplets [Martin *et al.*, 2008]. The trends in Z are consistent with studies of much larger silicate particles (i.e., Pele's tears, $d > 200 \mu\text{m}$) from Masaya [Moune *et al.*, 2007], which show that the maximum depth of alteration was $\sim 10 \mu\text{m}$. However, these larger particles were collected from the floor of the crater so it is possible that at least some of this alteration occurred after deposition. Figure 4 shows that for particles with $d > 6 \mu\text{m}$, a greater proportion than expected (on the basis of the general trend in Z) were found to be metal-poor, indicating that these

particles may have had a prolonged exposure to the plume. These results support the suggestion made in section 4.1.1 that some fraction of the largest particles may have been deposited and resuspended.

4.2. S-Rich Particles and Chlorides

[27] QEMSCAN analysis of particle filters may also be used to investigate the size distributions of other insoluble particles within volcanic plumes, such as reduced S-rich particles. Trace metals such as As, Cd, Tl, Pb, and Zn have a strong affinity for sulfur [e.g., Aiuppa *et al.*, 2003] and it is expected that reduced S-rich particles would be significantly enriched in these metals relative to other particles within Masaya's plume. Martin *et al.* [2008] show that $N(d)$ for reduced S-rich particles (e.g., sulfur and sulfides) in Mount Etna's plume decreases more rapidly with increasing particle size than $N(d)$ for fine silicate particles. An identical trend is found in the results from Masaya where the mass ratio of reduced S-rich particles to fine silicate particles decreases from 0.13 (at $d < 1 \mu\text{m}$) to 0.04 (at $d \sim 4 \mu\text{m}$). If we assume that the overall mass ratio at the time of sampling (~ 0.1) is approximately representative for the 2003 campaign (although no mechanistic correlation is implied), we estimate a mass flux of reduced S-rich particles of $\sim 5 \text{ kg d}^{-1}$. The steep gradient of the reduced S-rich particle size distribution is consistent with condensation and growth from a vapor phase [Giggenbach, 1987]:



Previous work [Martin *et al.*, 2008] shows that aqueous/soluble particles are undercounted by QEMSCAN analysis of particle filters (due to soaking into the filter). Hence, this technique cannot be used to assess the size distribution of sulfates (i.e., oxidized S-rich particles) or chlorides. A more appropriate technique for investigating the size distributions of soluble particles would be cascade impaction and ion chromatographic analysis [Mather *et al.*, 2003]. In spite of these limitations, QEMSCAN results indicate that the most abundant sulfate in Masaya's plume is Na-K sulfate with a smaller amount of Ca sulfate. These results are in agreement

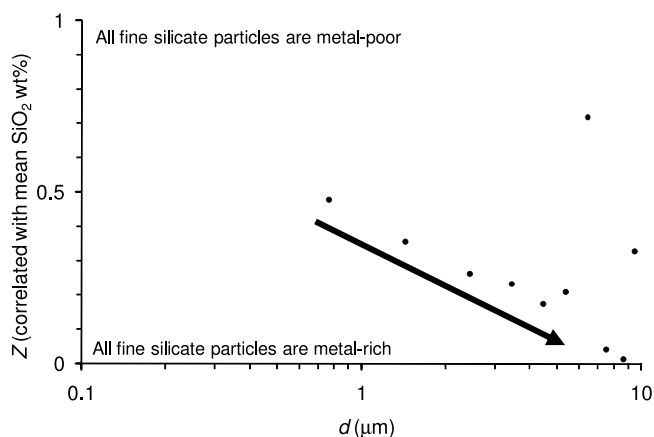


Figure 4. Z (which is positively correlated with SiO_2 wt%) against d for fine silicate particles in Masaya's plume (QM04). $Z = 1$ indicates that all fine silicate particles within the size interval had metal-poor compositions.

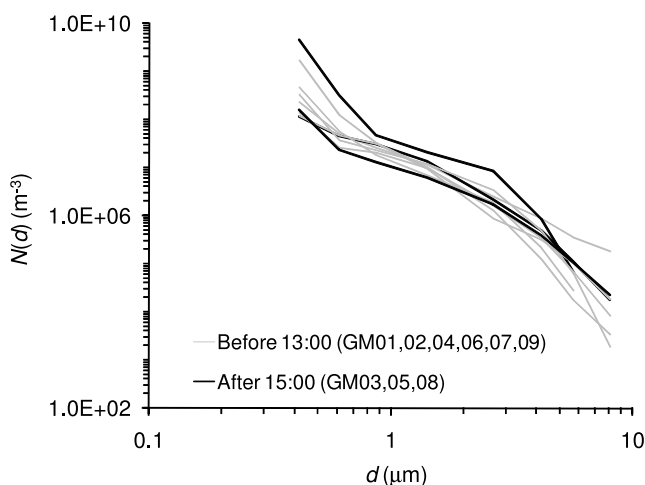


Figure 5a. Number density distribution, $N(d)$, from aerosol spectrometry, calculated as mean $N(d)$ within each sampling period (GM01–GM09). Measurements are grouped according to the time of day the measurements were taken. Standard errors of the mean due to analytical uncertainties are $< 4\%$.

with those of *Mather et al.* [2003] showing strong correlations between the size distributions of Na^+ , K^+ , and SO_4^{2-} in Masaya's plume. Negligible quantities of chloride were detected by QEMSCAN, despite there being a significant amount of chloride in Masaya's plume [*Mather et al.*, 2003]. This result reflects the lower abundance of chloride relative to sulfate in Masaya's plume ($\text{Cl}^-/\text{SO}_4^{2-} \sim 0.2$ [*Mather et al.*, 2003]), with a large fraction of Cl^- potentially being aqueous HCl (undetectable by QEMSCAN owing to soaking into the filter and/or evaporation under the near-vacuum conditions employed during analysis).

4.3. Particle Size Distributions From Other Techniques

[28] $N(d)$ from aerosol spectrometry was calculated from mean $N(d)$ within each sampling period (GM01–GM09) including measurements when the plume was not blowing over the measurement site. The same approach was used to calculate mean $C(d)$ from Sun photometry (SP01–SP04). The analytical uncertainties are small compared to the inherent variability due to plume dilution and puffing, and the standard errors of the mean due to analytical uncertainties are $< 4\%$ (for both techniques; Table 2).

[29] Aerosol spectrometry results ($N(d)$, GM01–GM09) are shown in Figure 5a. $N(d)$ generally decreases with increasing particle size. All samples show a shoulder at $\sim 1 \mu\text{m}$ which remains if $N(d)$ for the fine silicate particles is subtracted. The diurnal variation of Masaya's plume [*Mather et al.*, 2003] is evident with measurements taken later in the day (i.e., > 1500 ; GM03, GM05, GM08) showing increased $N(d)$ for the largest particles. Sun photometer results ($C(d)$, SP01–SP04) are shown in Figure 5b. Two of the four sampling periods (SP01 and SP04) show a local maximum in $C(d)$ at $\sim 1 \mu\text{m}$ with the remainder showing a shoulder at $\sim 1 \mu\text{m}$. SP01 and SP04 show a corresponding depletion at $\sim 0.5 \mu\text{m}$, which suggests that the $1\text{-}\mu\text{m}$ mode is formed by growth of smaller particles. Results from both techniques indicate that the size distribution of particles in Masaya's

plume is variable on time scales of hours. While some of this variability can be explained by temperature and relative humidity (e.g., diurnal variation leading to particle growth), it is not clear how these meteorological variables affect more specific variations in the size distribution (e.g., the observed variations in $C(d)$ at $\sim 1 \mu\text{m}$).

[30] The number of particles with $0.01 < d(\mu\text{m}) < 0.04$ (typically $\sim 10\text{--}50$) detected on each $\sim 4 \mu\text{m}^2$ of grid (TP01, TP02, and TP03) were too small to assess variation across the size range. However, if the range $0.01 < d(\mu\text{m}) < 0.04$ is taken as a single bin, we estimate (using equation (3b)) that $N(d) \sim 2 \times 10^{11} \text{ m}^{-3}$ at the crater rim. Future thermal precipitator studies of Masaya's plume (with instruments based on the work of *Maynard* [1995]) should employ longer measurement times (i.e., > 60 min) to ensure larger quantities of nanoparticles are collected.

4.4. Comparison of Size Distributions From All Techniques

[31] Figure 6 shows several determinations of $N(d)$ at the crater rim: $N(d)$ for fine silicate particles from QEMSCAN (QM04), mean $N(d)$ from aerosol spectrometry (for < 1300 and > 1500), and $N(d)$ from thermal precipitation. Also shown is $N(d)$ calculated from Sun photometer measurements (using equation (4), with the average plume thickness, $L = 32$ m) by taking the mean of 10 measurements of $C(d)$ with the highest total column particles, $C_{\text{tot}}(\text{m}^{-2})$, in each sampling period (SP01–SP04) (C_{tot} is obtained by integration of $C(d)$ over $0.08 < d(\mu\text{m}) < 4$). The filtered results for Sun photometry are approximately equivalent to $N(d)$ in the plume (averaged over the plume column) since measurements with little or no plume were excluded from the calculation. Mean $N(d)$ in background air measured by aerosol spectrometry is also shown.

[32] The shoulders at $1 \mu\text{m}$ for SP02 and SP03 (Figure 5b) are no longer apparent when only scans with high C_{tot} are considered, suggesting that during these sampling periods, plumes with low C_{tot} had an increased proportion of particles with $d \sim 1 \mu\text{m}$. In contrast, the $1\text{-}\mu\text{m}$ mode remains in SP01

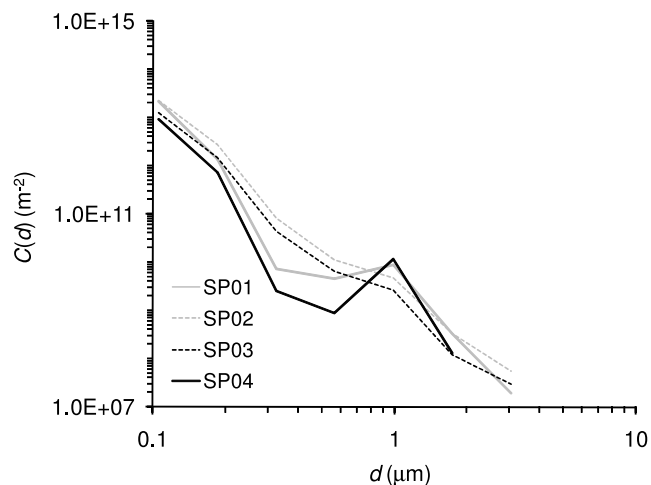


Figure 5b. Column number density distribution, $C(d)$, from Sun photometry, calculated as mean $C(d)$ over each sampling period (SP01–SP04). Standard errors of the mean due to analytical uncertainties are $< 4\%$.

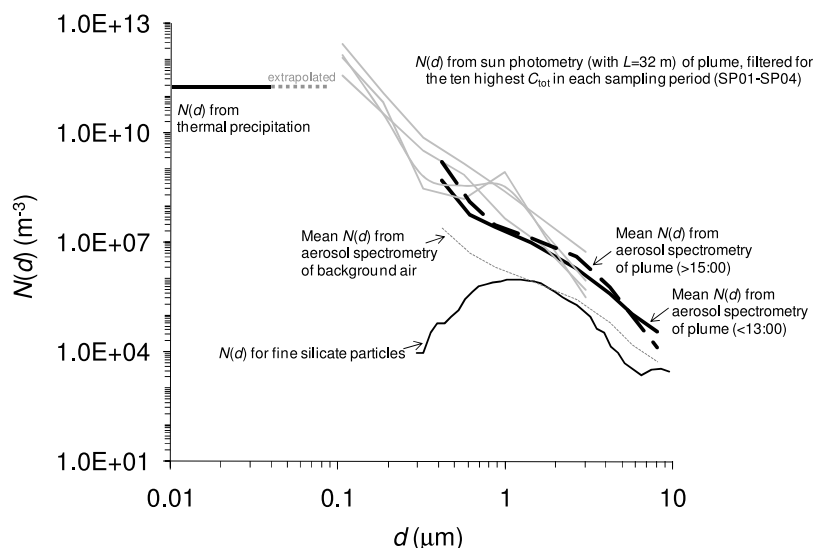


Figure 6. A comparison of number density distributions, $N(d)$, in Masaya's plume from different sampling and measurement techniques.

and SP04, indicating that the plume was more homogeneous during these sampling periods. The $1\text{-}\mu\text{m}$ mode is evident as a shoulder at $\sim 1\text{ }\mu\text{m}$ in aerosol spectrometry measurements. If the differences in prominence were a reflection of vertical heterogeneity in the plume, with the aerosol spectrometer only sampling the base of the plume (i.e., direct sampling) and Sun photometry sampling the whole column (i.e., remote sensing), this would imply that particles with $d \sim 1\text{ }\mu\text{m}$ are most concentrated at the top of the plume. While this spatial distribution of particles could imply the involvement of photochemistry or reactions involving reagents mixing in from the background atmosphere in particle formation, it is also possible that the two instruments would offer different results, even when sampling a uniform plume. Within both techniques, we are forced to assume spherical particles with a wavelength-independent index of refraction, and a constant atmospheric background (in the case of Sun photometry, along the entire atmospheric column). These assumptions are significant and may require further examination. Our results show that despite overall similarities (e.g., a mode at $d \sim 1\text{ }\mu\text{m}$ superimposed onto a power law distribution with $N(d) \propto d^{-3}$), there are differences in detail between the size distributions derived using aerosol spectrometry and Sun photometry.

[33] A mode at $\sim 1\text{ }\mu\text{m}$ is consistent with earlier studies of Masaya's plume. Allen *et al.* [2002] reported particulate H^+ and SO_4^{2-} in the plume of Masaya (measured in May 2001) to be concentrated in particles $< 2.5\text{ }\mu\text{m}$. Mather *et al.* [2003] sampled the plume of Masaya in December 2001 with a cascade impactor and showed that concentrations of Na^+ , K^+ , H^+ , and SO_4^{2-} peak at $\sim 0.5\text{ }\mu\text{m}$. Correspondence between the size distributions of Na^+ , K^+ , SO_4^{2-} , H^+ , and total particles indicates that sulfate particles in the plume are important heterogeneous condensation nuclei for water, forming aqueous droplets at $\sim 1\text{ }\mu\text{m}$. This result suggests that the formation of particles with $d \sim 1\text{ }\mu\text{m}$ may depend upon the concentration of "near-source" volcanic sulfates in the plume. While the origins of volcanic sulfate particles are not well understood, recent studies have suggested

that an important process in their formation is the high-T oxidation of SO_2 to SO_3 by atmospheric gases at the vent [Mather *et al.*, 2006b; Martin *et al.*, 2006]. Within this mechanism, there is scope for variability in the emission of sulfates (and hence, in the size distribution of particles in the plume) due to the unsteady dynamics of gas mixing at the vent.

[34] $N(d)$ for $0.01 < d\text{ (}\mu\text{m)} < 0.04$ (from thermal precipitation) is below $N(d)$ at $d \sim 0.1\text{ }\mu\text{m}$ (from Sun photometry). This difference reflects the filtering (i.e., the removal of measurements with low C_{tot}) applied to Sun photometry results. Additionally, the uncertainties on L are large. While we cannot exclude the possibility that $N(d)$ for $0.01 < d\text{ (}\mu\text{m)} < 0.04$ was different in 2006 from in 2003, the first two factors are more than sufficient to explain the observed differences in $N(d)$. We henceforth assume that there were no order of magnitude differences in the size distribution of particles between 2006 and 2003 (justified by the observations and measurements showing no significant differences in other aspects of the plume, e.g., SO_2 concentrations at the crater rim). Within this assumption, our results suggest that $N(d)$ does not increase significantly below $d \sim 0.1\text{ }\mu\text{m}$, and we may reasonably extrapolate $N(d)$ from thermal precipitation to $0.08\text{ }\mu\text{m}$ (to close the gap in the size distribution). The resultant size distribution is consistent with studies of Mount Etna's plumes where $N(d)$ was not found to vary significantly (particularly for the Voragine plume) across the $0.01 < d\text{ (}\mu\text{m)} < 0.1$ range [Martin *et al.*, 2008]. These results reflect particles in the nucleation mode ($d < 0.1\text{ }\mu\text{m}$) growing rapidly by coagulation, limiting $N(d)$ within this size range but increasing $N(d)$ within the accumulation mode ($0.1 < d\text{ (}\mu\text{m)} < 2$) [Whitby, 1978].

[35] Results show that $N(d)$ for silicate particles from the QEMSCAN was below $N(d)$ calculated from either aerosol spectrometry or Sun photometry but comparable to mean $N(d)$ in background air. No studies have been made to investigate the composition of background air in this region of Nicaragua. However, contributions from aqueous droplets, organic aerosols and carbonates [e.g., Hinds, 1999] are

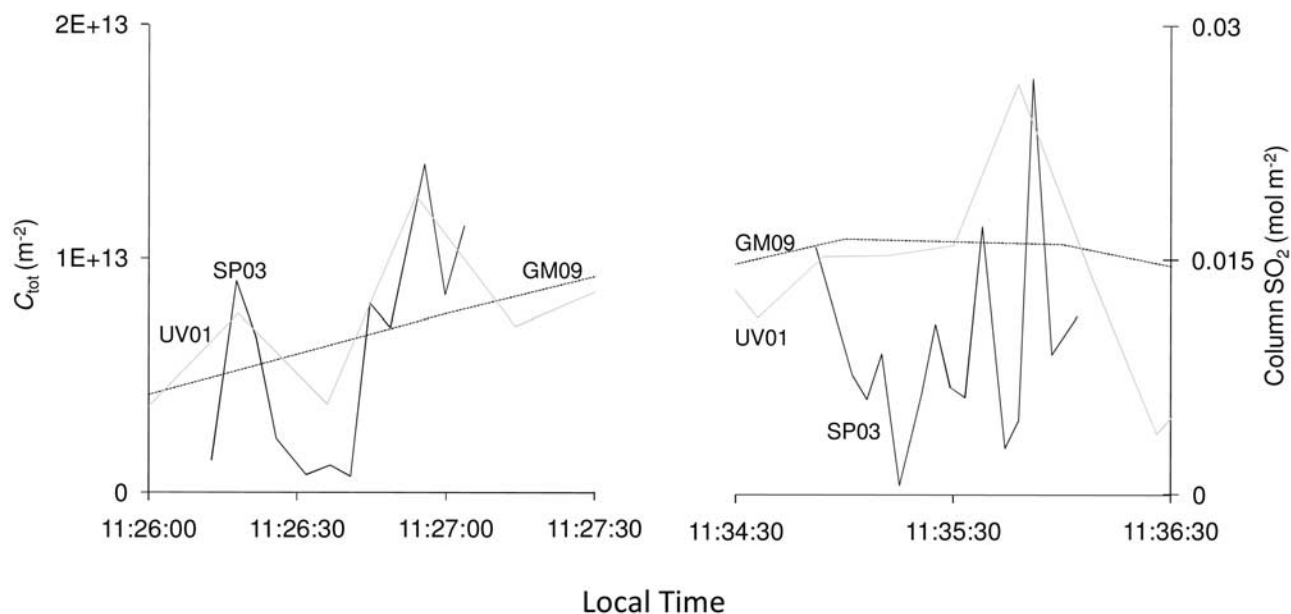


Figure 7. Time series showing total column particles (C_{tot}) from SP03 in parallel with differential optical absorption spectroscopy (DOAS) measurements of column SO_2 (UV01). Total particles (N_{tot}) from GM09 are shown with vertical scaling for clarity. Analytical uncertainties are $\sim 20\%$ for aerosol spectrometry, $\sim 10\%$ for Sun photometry, and $\sim 5\%$ for DOAS.

likely to be significant and the fine silicate particle background will be less than the indicated total. Moreover, given Masaya's geographic location (downwind of extensive rain forests and the Atlantic Ocean), we might reasonably expect the contribution of silicates to background air to be small. In any case, the spherical shape of fine silicate particles in Masaya's plume precludes significant contamination from atmospheric silicate dusts, which are generally more angular [e.g., Okada *et al.*, 2001].

4.5. Estimates of Total Particle Emission and Mass Fluxes

[36] Figure 7 shows good agreement between total column particles (C_{tot}) from Sun photometry (SP03) and column SO_2 (mol m^{-2}) measured using DOAS (UV01). Total particles (N_{tot} (m^{-3}); output directly by data-processing software over $0.35 < d (\mu\text{m}) < 10$) from aerosol spectrometry (GM09) is shown scaled (by 10^5) to give the best agreement with C_{tot} . The Sun was close to the zenith at the time of measurement (~ 1100 local time) so the lines of sight of DOAS (toward the zenith) and the Sun photometer (toward the Sun) were approximately equivalent. The correlation between column SO_2 and C_{tot} indicates that there is a limited amount of decoupling between the particles and gas in the plume at this stage of the plume's development. Aerosol spectrometry measurements are in agreement although the time interval between measurements (i.e., 1 min) is too long to assess rapid changes in the particle size distribution of the plume.

[37] Our results suggest mean column $\text{SO}_2 \sim 0.01 \text{ mol m}^{-2}$ (calculated from UV01). Taking this value as representative, we estimate mean $C_{\text{tot}}/\text{SO}_2$ (calculated from SP01–SP04) to be $\sim 5 \times 10^{14} \text{ mol}^{-1}$, which scaled by the emission

flux of SO_2 , gives an emission flux of $\sim 2 \times 10^{16} \text{ s}^{-1}$ where $0.08 < d (\mu\text{m}) < 4$. This emission flux is comparable to those previously calculated for Lascar ($\sim 10^{17} \text{ s}^{-1}$) and Villarrica ($\sim 10^{16} \text{ s}^{-1}$) using Sun photometry [Mather *et al.*, 2004c]. Furthermore, we integrate $N(d)$ (from thermal precipitation) and scale to estimate an emission flux of $\sim 4 \times 10^{16} \text{ s}^{-1}$ where $0.01 < d (\mu\text{m}) < 0.08$. The contribution of particles with $d > 4 \mu\text{m}$ to the total emission flux is negligible. Thus, we estimate a total emission flux from Masaya of $\sim 10^{17} \text{ s}^{-1}$.

[38] Mass fluxes were estimated by assuming that particles are dominated by a mixture of water and H_2SO_4 (density = 1670 kg m^{-3} [Mather *et al.*, 2004c]) and performing the appropriate manipulations of $C(d)$ or $N(d)$ (see section 3.3). The validity of the density value is not affected by the results of the present study; the total emission flux of particles exceeds that of the fine silicate particles by a factor of $\sim 10^6$ so the contribution of fine silicate particles to the average particle density is negligible. The mass flux from aerosol spectrometry (calculated from GM01–GM09) was estimated as $\sim 1 \text{ Mg d}^{-1}$ where $0.35 < d (\mu\text{m}) < 10$. The mass flux from Sun photometry (calculated from SP01–SP04) was estimated to be $\sim 5 \text{ Mg d}^{-1}$ where $0.08 < d (\mu\text{m}) < 4$. The mass flux from thermal precipitation (calculated from TP01–TP03) was estimated to be $\sim 0.5 \text{ Mg d}^{-1}$ where $d < 0.1 \mu\text{m}$. Previous work on Masaya's plume estimated an SO_4^{2-} flux of 6 Mg d^{-1} at the crater rim (as in the work of Mather *et al.* [2003], where the SO_2 emission flux was twice that of the current study). This earlier result lends support to using the sum of the mass fluxes derived using Sun photometry and thermal precipitation as the best estimate of the mass flux of particles from Masaya ($\sim 5.5 \text{ Mg d}^{-1}$ where $d < 4 \mu\text{m}$). If further

condensation occurs downwind of the crater rim, the “true” mass flux of particles from Masaya may be greater than our estimate.

5. Conclusions

[39] Volcanic plumes are a complex mixture of gas and particles which evolve over a range of time scales and any characterization study can only offer a “snapshot” of plume chemistry at a specific time. However, studies such as this may provide insights into the processes occurring at the magma surface and in the vent and crater immediately prior to measurements.

[40] QEMSCAN enables the detection and measurement of fine silicate particles in Masaya's volcanic plume. The size distribution of fine silicate particles was found to be approximately lognormal. This distribution is consistent with the fine silicate particles being produced by a single process, such as the bursting of gas bubbles at the surface of the magma. The fine silicate particles in Masaya's plume are significantly smaller and more spherical than fine silicate particles in the Mount Etna plume. Our analysis confirms earlier studies showing that fine silicate particles are compositionally variable, and that the extent of this compositional variability decreases with increasing particle size. The emission flux of fine silicate particles from Masaya was estimated to be $\sim 10^{11} \text{ s}^{-1}$, equivalent to $\sim 55 \text{ kg d}^{-1}$. The size, shape, and composition of fine silicate particles may provide useful information about preemission, synemission, and postemission processes during quiescent activity if further work allows us to understand their formation processes.

[41] Sun photometry, aerosol spectrometry, and thermal precipitation were used to calculate the size distribution for total particles in the plume over the size range $0.01 < d (\mu\text{m}) < 10$. Results from Sun photometry and aerosol spectrometry show a mode (either a local maximum, or shoulder in the size distribution) at $d \sim 1 \mu\text{m}$, which is observed in dense plumes in some sampling periods but only at the plume edges in others. Despite overall similarities, differences in detail were found between size distributions calculated from Sun photometry and aerosol spectrometry. The reasons for these differences are unclear at present. Results from Sun photometry and thermal precipitation are consistent and indicate high concentrations of nanoparticles in Masaya's plume. Using results from Sun photometry and thermal precipitation, we estimate the emission flux of particles from Masaya to be $\sim 10^{17} \text{ s}^{-1}$ and the mass flux of particles to be $\sim 5.5 \text{ Mg d}^{-1}$ where $d < 4 \mu\text{m}$.

[42] **Acknowledgments.** R. S. M. thanks the Natural Environment Research Council for a Ph.D. studentship, research costs, and travel support and Christ's College, Cambridge, for a Junior Research Fellowship. T. A. M. thanks the Royal Society, and D. M. P. thanks the Leverhulme Trust for financial support. R. S. M. thanks Pierre Delmelle and Marie Edmonds for their insightful comments on earlier versions of this work. The authors would also like to thank Melanie Witt, INETER, and the staff of the Parque Nacional Volcan Masaya for their much-appreciated assistance in the field in Nicaragua. The NERC Field Spectroscopy Facility is also thanked for arranging the loan of the MICROTOS II instrument and for advice about its operation. Three anonymous reviewers and Glyn Williams-Jones are thanked for their comments.

References

Abramoff, M. D., P. J. Magelhaes, and S. J. Ram (2004), Image processing with ImageJ, *Biophotonics Int.*, 11, 36–42.

- Aiuppa, A., G. Dongarra, M. Valenza, C. Federico, and G. Pecoraino (2003), Degassing of trace volatile metals during the 2001 eruption of Etna, in *Volcanism and the Earth's Atmosphere*, *Geophys. Monogr. Ser.*, vol. 139, edited by A. Robock and C. Oppenheimer, pp. 41–44, AGU, Washington, D. C.
- Allen, A. G., C. Oppenheimer, M. Ferm, P. J. Baxter, L. A. Horrocks, B. Galle, A. J. S. McGonigle, and H. J. Duffell (2002), Primary sulfate aerosol and associated emissions from Masaya Volcano, Nicaragua, *J. Geophys. Res.*, 107(D23), 4682, doi:10.1029/2002JD002120.
- Allen, A. G., T. A. Mather, A. J. S. McGonigle, A. Aiuppa, P. Delmelle, B. Davison, N. Bobrowski, C. Oppenheimer, D. M. Pyle, and S. Inguaggiato (2006), Sources, size distribution, and downwind grounding of aerosols from Mount Etna, *J. Geophys. Res.*, 111, D10302, doi:10.1029/2005JD006015.
- Baxter, P. J., R. E. Stoiber, and S. N. Williams (1982), Volcanic gases and health: Masaya Volcano, Nicaragua, *Lancet*, 320(8290), 150–151, doi:10.1016/S0140-6736(82)91109-6.
- Branan, Y. K., A. J. Harris, I. M. Watson, J. C. Phillips, K. Horton, G. Williams-Jones, and H. Garbeil (2008), Investigation of at-vent dynamics and dilution using thermal infrared radiometers at Masaya volcano, Nicaragua, *J. Volcanol. Geotherm. Res.*, 169(1–2), 34–37, doi:10.1016/j.jvolgeores.2007.07.021.
- Burton, M. R., C. Oppenheimer, L. A. Horrocks, and P. W. Francis (2000), Remote sensing of CO_2 and H_2O emission rates from Masaya volcano, Nicaragua, *Geology*, 28, 915–918, doi:10.1130/0091-7613(2000)28<915:RSOAH>2.0.CO;2.
- Delmelle, P., J. Stix, C. P. A. Bourque, P. J. Baxter, J. Garcia-Alvarez, and J. Barquero (2001), Dry deposition and heavy acid loading in the vicinity of Masaya volcano, a major sulfur and chlorine source in Nicaragua, *Environ. Sci. Technol.*, 7, 1289–1293.
- Delmelle, P., J. Stix, P. J. Baxter, J. Garcia-Alvarez, and J. Barquero (2002), Atmospheric dispersion, environmental effects and potential health hazard associated with the low-altitude gas plume of Masaya volcano, Nicaragua, *Bull. Volcanol.*, 64, 423–434, doi:10.1007/s00445-002-0221-6.
- Delmelle, P., M. Lambert, Y. Dufrene, P. Gerin, and N. Oskarsson (2007), Gas/aerosol-ash interaction in volcanic plumes: New insights from surface analyses of fine volcanic ash, *Earth Planet. Sci. Lett.*, 259, 159–170, doi:10.1016/j.epsl.2007.04.052.
- Duffell, H. J., C. Oppenheimer, D. M. Pyle, B. Galle, A. J. S. McGonigle, and M. R. Burton (2003), Changes in gas composition prior to a minor explosive eruption at Masaya volcano, Nicaragua, *J. Volcanol. Geotherm. Res.*, 126, 327–339, doi:10.1016/S0377-0273(03)00156-2.
- Galle, B., C. Oppenheimer, A. Geyer, A. J. S. McGonigle, M. Edmonds, and L. Horrocks (2003), A miniaturised ultraviolet spectrometer for remote sensing of SO_2 fluxes: A new tool for volcano surveillance, *J. Volcanol. Geotherm. Res.*, 119(1–4), 241–254, doi:10.1016/S0377-0273(02)00356-6.
- Giggenbach, W. F. (1987), Redox processes governing the chemistry of fumarolic gas discharges from White Island, New Zealand, *Appl. Geochem.*, 2, 143–161, doi:10.1016/0883-2927(87)90030-8.
- Han, Z. J., and L. Holappa (2001), Formation of metal droplets from gas bubbles bursting on iron melt, *Steel Res.*, 72, 434–438.
- Han, Z. J., and L. Holappa (2003), Bubble bursting phenomenon in gas/metal/slag systems, *Metall. Mater. Trans. B*, 34, 525–532, doi:10.1007/s11663-003-0020-2.
- Hinds, W. C. (1999), *Aerosol Technology: Properties, Behavior, and Measurement of Airborne Particles*, 483 pp., John Wiley, New York.
- Horrocks, L., M. Burton, P. Francis, and C. Oppenheimer (1999), Stable gas plume composition measured by OP-FTIR spectroscopy at Masaya Volcano, Nicaragua, 1998–1999, *Geophys. Res. Lett.*, 26(23), 3497–3500, doi:10.1029/1999GL008383.
- Horwell, C. J. (2007), Grain-size analysis of volcanic ash for the rapid assessment of respiratory health hazard, *J. Environ. Monit.*, 9, 1107–1115, doi:10.1039/b710583p.
- Horwell, C. J., and P. J. Baxter (2006), The respiratory health hazards of volcanic ash: A review for volcanic risk mitigation, *Bull. Volcanol.*, 69, 1–24, doi:10.1007/s00445-006-0052-y.
- King, M. D. (1982), Sensitivity of constrained linear inversions to the selection of the Lagrange multiplier, *J. Atmos. Sci.*, 39(6), 1356–1369, doi:10.1175/1520-0469(1982)039<1356:SOCLIT>2.0.CO;2.
- Lefevre, R., A. Gaudichet, and M. A. Billon-Galand (1986), Silicate microspherules intercepted in the plume of Etna volcano, *Nature*, 322, 817–820, doi:10.1038/322817a0.
- Lewis, E. R., and S. E. Schwartz (2004), *Sea Salt Aerosol Production: Mechanisms, Methods, Measurements, and Models: A Critical Review*, *Geophys. Monogr. Ser.*, vol. 152, 413 pp., AGU, Washington, D. C.
- Martin, R. S., T. A. Mather, and D. M. Pyle (2006), High-temperature mixtures of magmatic and atmospheric gases, *Geochem. Geophys. Geosyst.*, 7, Q04006, doi:10.1029/2005GC001186.

- Martin, R. S., T. A. Mather, D. M. Pyle, M. Power, A. G. Allen, A. Aiuppa, C. J. Horwell, and E. P. W. Ward (2008), Composition-resolved size distributions of volcanic aerosols in the Mt. Etna plumes, *J. Geophys. Res.*, **113**, D17211, doi:10.1029/2007JD009648.
- Martinez-Lozano, J. A., M. P. Utrillas, and F. Tena (1999), Retrieval of the aerosol size distribution from spectroradiometer measurements at a coastal site in the Mediterranean Sea, *Int. J. Remote Sens.*, **20**(11), 2167–2182, doi:10.1080/014311699212173.
- Mather, T. A., A. G. Allen, C. Oppenheimer, D. M. Pyle, and A. J. S. McGonigle (2003), Size-resolved characterisation of soluble ions in the particles in the tropospheric plume of Masaya volcano, Nicaragua: Origins and plume processing, *J. Atmos. Chem.*, **46**, 207–237, doi:10.1023/A:1026327502060.
- Mather, T. A., A. G. Allen, B. M. Davison, D. M. Pyle, C. Oppenheimer, and A. J. S. McGonigle (2004a), Nitric acid from volcanoes, *Earth Planet. Sci. Lett.*, **218**(1–2), 17–30, doi:10.1016/S0012-821X(03)00640-X.
- Mather, T. A., D. M. Pyle, and A. G. Allen (2004b), Volcanic source for fixed nitrogen in the early Earth's atmosphere, *Geology*, **32**(10), 905–908, doi:10.1130/G20679.1.
- Mather, T. A., V. I. Tsanev, D. M. Pyle, A. J. S. McGonigle, C. Oppenheimer, and A. G. Allen (2004c), Characterization and evolution of tropospheric plumes from Lascar and Villarica volcanoes, Chile, *J. Geophys. Res.*, **109**, D21303, doi:10.1029/2004JD004934.
- Mather, T. A., D. M. Pyle, V. I. Tsanev, A. J. S. McGonigle, C. Oppenheimer, and A. G. Allen (2006a), A reassessment of current volcanic emissions from the Central American arc with specific examples from Nicaragua, *J. Volcanol. Geotherm. Res.*, **149**, 297–311, doi:10.1016/j.jvolgeores.2005.07.021.
- Mather, T. A., J. R. McCabe, V. K. Rai, M. H. Thiemens, D. M. Pyle, T. H. E. Heaton, H. J. Sloane, and G. R. Fern (2006b), Oxygen and sulfur isotopic composition of volcanic sulfate aerosol at the point of emission, *J. Geophys. Res.*, **111**, D18205, doi:10.1029/2005JD006584.
- Maynard, A. D. (1995), The development of a new thermophoretic precipitator for scanning-transmission electron-microscope analysis of ultra-fine aerosol-particles, *Aerosol Sci. Technol.*, **23**, 521–533, doi:10.1080/02786829508965334.
- McGonigle, A. J. S., C. Oppenheimer, B. Galle, T. A. Mather, and D. M. Pyle (2002), Walking traverse and scanning DOAS measurements of volcanic gas emission rates, *Geophys. Res. Lett.*, **29**(20), 1985, doi:10.1029/2002GL015827.
- McGonigle, A. J. S., C. Oppenheimer, A. R. Hayes, B. Galle, M. Edmonds, T. Caltabiano, G. Salerno, M. Burton, and T. A. Mather (2003), Sulphur dioxide fluxes from Mount Etna, Vulcano, and Stromboli measured with an automated scanning ultraviolet spectrometer, *J. Geophys. Res.*, **108**(B9), 2455, doi:10.1029/2002JB002261.
- Meeker, G. P., and T. K. Hinkley (1993), The structure and composition of microspheres from the Kilauea volcano, Hawaii, *Am. Mineral.*, **78**, 873–876.
- Morys, M., F. M. Mims III, S. Hagerup, S. E. Anderson, A. Baker, J. Kia, and T. Walkup (2001), Design, calibration, and performance of MICROTOPS II handheld ozone monitor and Sun photometer, *J. Geophys. Res.*, **106**(D13), 14,573–14,582, doi:10.1029/2001JD900103.
- Moune, S., F. Francois, P. J. Gauthier, and K. W. W. Sims (2007), Pele's hairs and tears: Natural probe for volcanic plume, *J. Volcanol. Geotherm. Res.*, **164**(4), 244–253, doi:10.1016/j.jvolgeores.2007.05.007.
- Obenholzer, J. H., H. Schroettner, P. Golob, and H. Delgado (2003), Particles from the plume of Popocatepetl volcano, Mexico: The FESEM/EDS approach, in *Volcanic Degassing*, edited by C. Oppenheimer, D. M. Pyle, and J. Barclay, *Geol. Soc. Spec. Publ.*, vol. 213, pp. 123–148.
- Okada, K., J. Heintzenberg, K. Kai, and Y. Qin (2001), Shape of atmospheric mineral particles collected in three Chinese arid-regions, *Geophys. Res. Lett.*, **28**(16), 3123–3126, doi:10.1029/2000GL012798.
- Pfeffer, M. A., F. J. M. Rietmeijer, A. J. Brearley, and T. P. Fischer (2006), Electron microbeam analyses of aerosol particles from the plume of Poás Volcano, Costa Rica, and comparison with equilibrium plume chemistry modeling, *J. Volcanol. Geotherm. Res.*, **152**(1–2), 174–188, doi:10.1016/j.jvolgeores.2005.10.009.
- Pirrie, D., A. R. Butcher, M. R. Power, P. Gottlieb, and G. L. Miller (2004), Rapid quantitative mineral and phase analysis using automated scanning electron microscopy (QemSCAN): Potential applications in forensic geoscience, in *Forensic Geoscience: Principles, Techniques and Applications*, edited by K. Pye and D. J. Croft, *Geol. Soc. Spec. Publ.*, vol. 232, pp. 123–136.
- Pirrie, D., M. R. Power, G. K. Rollinson, P. E. J. Wiltshire, J. Newberry, and H. E. Campbell (2009), Automated SEM-EDS (QEMSCAN) mineral analysis in forensic soil investigations: Testing instrumental reproducibility, in *Criminal and Environmental Soil Forensics*, edited by K. Ritz, L. Dawson, and D. Miller, pp. 411–430, Springer, New York.
- Polacci, M., R. A. Corsaro, and D. Andronico (2006), Coupled textural and compositional characterization of basaltic scoria: Insights into the transition from Strombolian to fire fountain activity at Mount Etna, Italy, *Geology*, **34**, 201–204, doi:10.1130/G22318.1.
- Porter, J. N., K. A. Horton, P. J. Mouginiis-Mark, B. Lienert, S. K. Sharma, E. Lau, A. J. Sutton, T. Elias, and C. Oppenheimer (2002), Sun photometer and lidar measurements of the plume from the Hawaii Kilauea Volcano Pu'u O'o vent: Aerosol flux and SO₂ lifetime, *Geophys. Res. Lett.*, **29**(16), 1783, doi:10.1029/2002GL014744.
- Russell, L. M., and E. G. Singh (2006), Submicron salt particle production in bubble bursting, *Aerosol Sci. Technol.*, **40**, 664–671, doi:10.1080/02786820600793951.
- Rymer, H., B. V. de Vries, J. Stix, and G. Williams-Jones (1998), Pit crater structure and processes governing persistent activity at Masaya Volcano, Nicaragua, *Bull. Volcanol.*, **59**, 345–355, doi:10.1007/s004450050196.
- Spadaro, F. R., R. A. Lefevre, and P. Ausset (2002), Experimental rapid alteration of basaltic glass: Implications for the origins of atmospheric particulates, *Geology*, **30**, 671–674, doi:10.1130/0091-7613(2002)030<0671:ERAOBG>2.0.CO;2.
- Spiel, D. E. (1998), On the births of film drops from bubbles bursting on seawater surfaces, *J. Geophys. Res.*, **103**(C11), 24,907–24,918, doi:10.1029/98JC02233.
- Stoiber, R. E., S. N. Williams, and B. J. Huebert (1986), Sulfur and halogen gases at Masaya caldera complex, Nicaragua: Total flux and variations with time, *J. Geophys. Res.*, **91**(B12), 12,215–12,231, doi:10.1029/JB091iB12p12215.
- Taddeucci, J., M. Pompilio, and P. Scarlato (2004), Conduit processes during the July August 2001 explosive activity of Mt. Etna (Italy): Inferences from glass chemistry and crystal size distribution of ash particles, *J. Volcanol. Geotherm. Res.*, **137**(1–3), 33–54, doi:10.1016/j.jvolgeores.2004.05.011.
- Taddeucci, J., P. Scarlato, D. Andronico, A. Cristaldi, R. Büttner, B. Zimanowski, and U. Küppers (2007), Advances in the study of volcanic ash, *Eos Trans. AGU*, **88**(24), doi:10.1029/2007EO240001.
- Watson, I. M., and C. Oppenheimer (2000), Particle size distributions of Mount Etna's aerosol plume constrained by Sun photometry, *J. Geophys. Res.*, **105**(D8), 9823–9829, doi:10.1029/2000JD900042.
- Watson, I. M., and C. Oppenheimer (2001), Photometric observations of Mt. Etna's different aerosol plumes, *Atmos. Environ.*, **35**, 3561–3572, doi:10.1016/S1352-2310(01)00075-9.
- Whitby, K. T. (1978), The physical characteristics of sulfur aerosols, *Atmos. Environ.*, **12**, 135–159, doi:10.1016/0004-6981(78)90196-8.
- Witt, M. L. I., T. A. Mather, D. M. Pyle, A. Aiuppa, E. Bagnato, and V. I. Tsanev (2008), Mercury and halogen emissions from Masaya and Telica volcanoes, Nicaragua, *J. Geophys. Res.*, **113**, B06203, doi:10.1029/2007JB005401.
- Wohletz, K. H., and R. G. McQueen (1984), Volcanic and stratospheric dust-like particles produced by experimental water-melt interactions, *Geology*, **12**, 591–594, doi:10.1130/0091-7613(1984)12<591:VASDPP>2.0.CO;2.
- Zimanowski, B., K. Wohletz, P. Dellino, and R. Büttner (2003), The volcanic ash problem, *J. Volcanol. Geotherm. Res.*, **122**(1–2), 1–5, doi:10.1016/S0377-0273(02)00471-7.

A. G. Allen, Analytical Chemistry Department, Chemistry Institute, Sao Paulo State University, 14800-900 Araraquara, SP, Brazil.

C. J. Horwell, Institute of Hazard and Risk Research, Department of Earth Sciences, Durham University, South Road, Durham DH1 3LE, UK.

R. S. Martin, Department of Earth Sciences, University of Cambridge, Downing Street, Cambridge CB2 3EQ, UK. (rsm45@cam.ac.uk)

T. A. Mather and D. M. Pyle, Department of Earth Sciences, University of Oxford, Parks Road, Oxford OX1 3PR, UK.

C. Oppenheimer and V. I. Tsanev, Department of Geography, University of Cambridge, Downing Place, Cambridge CB2 3EN, UK.

M. Power, Intellection U.K. Ltd., Conwy LL22 8LJ, UK.

E. P. W. Ward, Department of Materials Science and Metallurgy, University of Cambridge, Pembroke Street, Cambridge CB2 3QZ, UK.